IEEE Access
Multidisciplinary | Rapid Review | Open Access Journal

Received November 30, 2019, accepted December 21, 2019, date of publication December 25, 2019,
date of current version January 6, 2020.

Digital Object Identifier 10.1109/ACCESS.2019.2962314

CZT Algorithm for Multiple-Receiver Synthetic Aperture Sonar

MENGBO MA, JINSONG TANG, AND HEPING ZHONG
Naval Institute of Underwater Acoustic Technology, Naval University of Engineering, Wuhan 430033, China
Corresponding author: Jinsong Tang (jinsongtangwh@163.com)

This work was supported in part by the National Natural Science Foundation of China under Grant 61671461.

ABSTRACT The compensation of slant range motion errors needs to be carried out after range pulse compression in the signal processing of multiple-receiver synthetic aperture sonar (SAS). Whereas range pulse compression cannot be performed as the first step in multiple-receiver SAS chirp scaling (CS) algorithm, as it requires the transmitted signal to be linearly frequency modulated. For this reason, it is difficult to combine CS algorithm with motion compensation. Besides, those imaging algorithms based on interpolation, such as range-Doppler algorithm and wavenumber domain algorithm, have plenty of computation load and large phase errors. Aimed at these problems, a CZT algorithm for multiple-receiver SAS in the non-stop-hop-stop mode is proposed in this paper. The proposed algorithm can correct range cell migration utilizing chirp-z transform, which avoids interpolation. Furthermore, the algorithm is easily combined with motion compensation as it can process pulse-compressed data directly. This paper describes the algorithm in 9 key steps, including the principle of correcting range cell migration utilizing chirp-z transform in discrete domain. In the simulation and sea trial data processing, the proposed algorithm provides image quality equal to the CS algorithm, and the algorithm is slightly more efficient than CS algorithm when combined with motion compensation.

INDEX TERMS Synthetic aperture sonar, multiple-receiver, CZT algorithm, motion compensation.

I. INTRODUCTION

Synthetic aperture sonar (SAS) utilizes a uniform linear motion of small physical aperture along the azimuth direction to create a large virtual aperture [1]. However, due to the wave, surge and the instability of sonar platform, it is difficult for sonar platform to maintain uniform linear motion in ocean environment [2], which results in motion errors. In a standard motion compensation procedure, the slant range motion errors need to be corrected after range pulse compression.

Synthetic aperture techniques originated in radar field [3]. In order to overcome the conflict between high azimuth resolution and useful mapping rate, practical SAS generally applies a single-transmitter, multiple-receiver system [3], [4]. However, the basic image reconstruction algorithms in SAS are still adapted from synthetic aperture radar (SAR) analog. Up to now, the proposed block algorithms for multiple-receiver SAS are mainly divided into three categories [5], [6]: rang-Doppler (RD) algorithm [7]–[10], chirp scaling (CS) algorithm [11]–[13] and wavenumber domain (ωK) algorithm [14]–[16].

Among these three kinds of algorithms, CS algorithm has the highest efficiency and phase preserving ability [17], [18]. However CS algorithm requires that the transmitted signal be a linear frequency modulated (LFM) signal [19], and when motion compensation is performed, it is necessary to implement range pulse compression first, and then decompress the signal, which reduces the efficiency of the algorithm. RD algorithm and ωK algorithm can process the signal after range pulse compression directly, but these algorithms need interpolation to complete range cell migration correction (RCMC), which leads to plenty of computation and phase errors [5]. In SAR, another two-dimensional frequency domain algorithm called chirp-z transform (CZT) algorithm has been proposed [20]–[23]. This algorithm realizes RCMC by chirp-z transform in two-dimensional frequency domain, which can process a non-LFM signal and pulse-compressed data, and the efficiency of the algorithm is quite high. So this paper studies the CZT algorithm for multiple-receiver SAS.

Firstly, the precise range history model of multiple-receiver SAS in non-stop-hop-stop mode is presented and the

The associate editor coordinating the review of this manuscript and approving it for publication was Eduardo Rosa-Molinar.

approximate range history is obtained with some approximations. Then the principle of RCMC utilizing chirp-z transform is analysed in discrete domain. Finally, the flow chart of CZT algorithm for multiple-receiver SAS is derived. The first step is compensating the phase errors introduced by non-stop-hop-stop mode and separate transducers for transmission and reception. The second step is converting the signal of multiple-receiver into the monostatic SAS equivalents by arranging the signal in the azimuth direction [24]. The last step is processing the signal with the monostatic CZT algorithm to obtain the focused image, but the azimuth walk caused by the non-stop-hop-stop mode needs to be corrected before the azimuth IFFT, which is an additional procedure. As the CS algorithm provides image quality equal to or better than RD algorithm [19], [25], the CZT algorithm is compared with the CS algorithm in the point target simulation and sea trial data processing. Quantitative measures show that the accuracy of the proposed algorithm is comparable to that of the multiple-receiver SAS CS algorithm [24]. As far as efficiency is concerned, the CZT algorithm for multiple-receiver SAS is lower than that of the CS algorithm for multiple-receiver SAS. However when the imaging algorithms are combined with motion compensation procedure in the multiple-receiver SAS, decompression processing is needed if CS algorithm is adopted, while CZT algorithm can process the signals after range pulse compression directly. In this case, CZT algorithm is more efficient than CS algorithm. So CZT algorithm is suitable for motion compensation in multiple-receiver SAS. Since this paper focuses on the CZT algorithm for multiple-receiver SAS, it does not include the motion compensation procedure, which has been preliminary studied in [26], but further research is needed.

The contents of this paper are as follows: Section II gives the precise range history model and its approximate expression of multiple-receiver SAS. In Section III, the CZT algorithm flow for multiple-receiver SAS is derived. The effectiveness of the proposed algorithm is demonstrated with the point target simulation and the sea trial data processing in Section IV. The last section summarizes the paper.

II. THE ECHO MODEL OF MULTIPLE-RECEIVER SAS

The imaging geometry model of multiple-receiver SAS system is shown in Fig. 1. The sonar platform moves along the x axis with a uniform velocity v, and the coordinates of the scene are defined as: the r axis represents the range direction (scatterer orthogonal distance from the velocity v), and the x axis represents the azimuth direction (scatterer location along the velocity v).

Assume that the arbitrary point scatterer in the scene is located at $(r, 0)$. The distance between the transmitter and the scatterer, and the distance between the ith receiver and the scatterer can be expressed respectively as

$$R_t(t; r) = \sqrt{(vt)^2 + r^2} \tag{1}$$

$$R_{r,i}(t; r) = \sqrt{(vt + v\tau_i* + u_i)^2 + r^2} \tag{2}$$

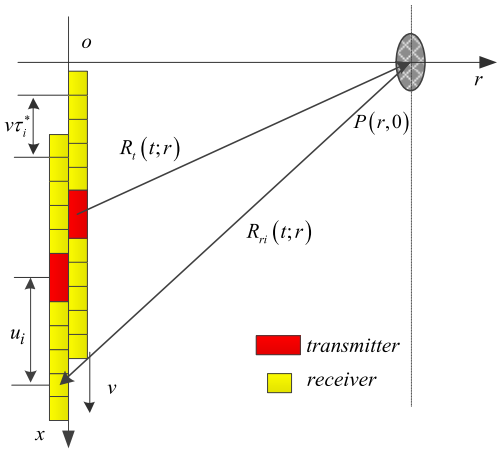

FIGURE 1. The geometry of multiple-receiver SAS.

where τ_i^* is the signal round-trip propagation time of the ith receiver, and u_i is the distance between transmitter and the ith receiver.

So the round-trip range history has the form

$$\begin{aligned} R_i(t; r) &= R_t(t; r) + R_{r,i}(t; r) \\ &= \sqrt{(vt)^2 + r^2} + \sqrt{(vt + v\tau_i^* + u_i)^2 + r^2} \end{aligned} \tag{3}$$

Assuming that the transmitted signal is a LFM pulse signal, the baseband form of the echo signal received by the ith receiver can be expressed as

$$\begin{aligned} ss_i(\tau, t; r) = A\omega_r(\tau)\omega_a(t)\exp[-j2\pi f_0 R_i(t; r)/c] \\ \times \exp\{j\pi K_r[\tau - R_i(t; r)/c]^2\} \end{aligned} \tag{4}$$

where f_0 is the center frequency, c is the speed of sound in the water, and K_r is the chirp rate of the transmitted signal. The functions $\omega_r(\tau)$ and $\omega_a(t)$ are transmitted signal envelope and azimuth antenna weighting, respectively. A represents the magnitude term of the echo signal, and if there is no special explanation, the latter formulas omit the magnitude term, which has nothing to do with the image quality.

According to [27], [28], the analytic expression of τ_i^* can be derived, here we rewrite it as (5) shown, at the bottom of the next page.

In order to get the approximate expression of (3), considering that the distance of the platform has moved along the azimuth is slowly changing, the signal round-trip propagation time τ_i^* in (3) can be approximated as that at center beam [24], i.e. $\tau_i^* = 2r/c$. So the round-trip range history can be approximated as

$$R_i(t; r) = \sqrt{(vt)^2 + r^2} + \sqrt{(vt + v\frac{2r}{c} + u_i)^2 + r^2} \tag{6}$$

Equation (6) can be further approximated [24] as

$$R_i(t; r) \approx 2RI(t; r) + \delta R(r) \tag{7}$$

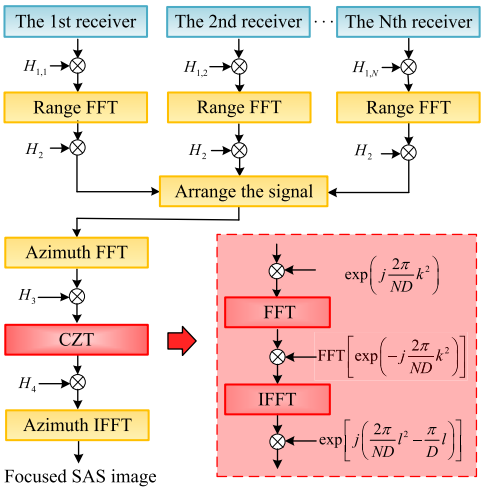

FIGURE 2. Flow diagram of multiple-receiver SAS processing algorithm based on the CZT procedure.

where $RI(t; r)$ is the distance between the phase center and the scatterer [9], [29], [30], i.e.

$$RI(t; r) = \sqrt{r^2 + (vt + v\frac{r}{c} + \frac{u_i}{2})^2} \tag{8}$$

and $\delta R(r)$ represents the high-order errors of range position caused by the non-stop-hop-stop mode and separate transducers for transmission and reception, i.e.

$$\delta R(r) = \frac{(v\frac{2r}{c} + u_i)^2}{4r} \tag{9}$$

The high-order errors of range position $\delta R(r)$ may impact both the phase and the envelope location of the signal impulse response (4), so the corresponding phase errors and time delay errors must be compensated in the preprocessing stage.

III. ALGORITHM PROCEDURE

Rather than correcting the differential range cell migration first like CS algorithm, the CZT algorithm completes the bulk RCMC first by a phase multiplication, which is the range-independent component of the range cell migration effect [23]. Then the differential range cell migration is corrected by chirp-z transform. So the RCMC procedure of CZT algorithm and that of CS algorithm are reversed.

The flow diagram of multiple-receiver SAS processing algorithm based on the CZT procedure is shown in Fig. 2. In the following, we will discuss the multiple-receiver SAS CZT algorithm in 9 key steps.

A. COMPENSATE THE HIGH-ORDER PHASE ERRORS

High-order phase errors caused by the non-stop-hop-stop mode and separate transducers for transmission and reception are compensated in this step. The high-order phase errors of each receiver are different, which need to be compensated with different phase term. For the ith receiver, the high-order phase errors can be compensated by multiplying a phase term

$$H_{1,i} = \exp[j2\pi f_0 \delta R(r)/c] \tag{10}$$

Then the echo signal of the ith receiver can be written as

$$ss_i'(\tau, t; r) = \omega_r(\tau)\omega_a(t)\exp[-j4\pi f_0 RI(t; r)/c] \times \exp\{j\pi K_r[\tau - R_i(t; r)/c]^2\} \tag{11}$$

B. RANGE FFT

According to the principle of stationary phase, the echo signal shown in (11) is transformed to range Doppler domain, which can be written as

$$Ss_i'(f_r, t; r) = W_r(f_r)\omega_a(t)\exp[-j4\pi f_0 RI(t; r)/c] \times \exp(-j\pi f_r^2/K_r)\exp[-j2\pi f_r R_i(t; r)/c] \tag{12}$$

where f_r is the frequency variable corresponding to range time and $W_r(f_r)$ is the Fourier transform of the pulse envelope.

C. COMPENSATE THE TIME DELAY ERRORS

The high-order errors of range position $\delta R(r)$, or the corresponding time delay errors $\delta R(r)/c$, can be measured by range resolution cell $\rho_r = C/2B_r$, so it depends on the velocity v, slant range r, the distance between receiver and transmitter u_i and the bandwidth of transmitted signal B_r. If the high-order errors of range position in the whole swath vary with range more than a range resolution cell, compensation should be performed using interpolation or small range blocks, which is usually encountered in motion compensation. If those errors vary with range less than a range resolution cell, compensation can be performed with reference range. Certainly, the high-order errors of range position can be neglected if less than a range resolution cell at reference range.

TABLE 1. Simulation parameters.

Parameter	Value
Center frequency	70kHz
Chirp duration	25ms
Chirp bandwidth	20kHz
Number of receiver	36
Platform velocity	2.5m/s
Pulse repetition interval (PRI)	0.576s
Length of transmitter	0.16m
Length of receiver	0.08m
Swath width (slant range)	60m-400m
Reference range	230m

$$\tau_i^* = \frac{c\sqrt{(vt)^2 + r^2} + v(vt + u_i) + \sqrt{[c\sqrt{(vt)^2 + r^2} + v(vt + u_i)]^2 + u_i(c^2 - v^2)(2vt + u_i)}}{c^2 - v^2} \tag{5}$$

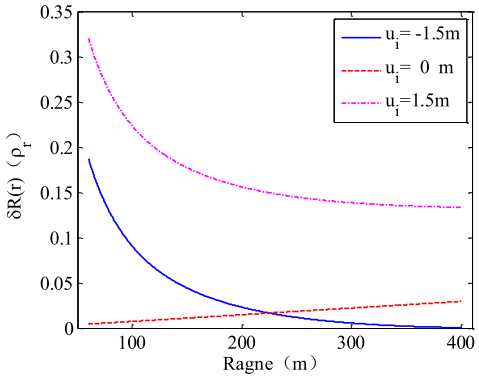

FIGURE 3. The high-order errors of range position of different receivers.

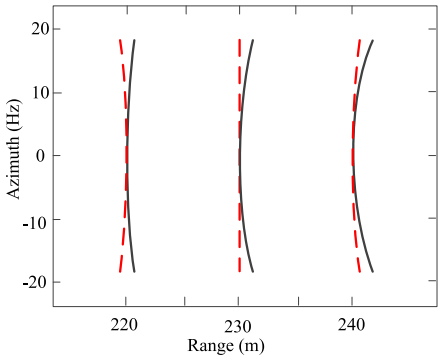

FIGURE 4. The signal trajectories in the range Doppler domain after bulk RCMC.

To analyze the time delay errors, we present some simulation results and the simulation parameters are shown in Table 1. Without losing generality, set the distance between the transmitter and the receiver as -1.5m, 0m and 1.5m. The simulation results are shown in Fig. 3.

We observed from Fig. 3 that the high-order errors of range position vary with range much less than a range resolution cell, and those at the reference range are also much less than a range resolution cell, so the high-order errors of range position introduced by the non-stop-hop-stop mode and separate transducers for transmission and reception can be neglected.

To implement range pulse compression directly, the reference function is

$$H_2 = \exp(j\pi f_r^2 \Big/ K_r) \tag{13}$$

The signal after neglecting the high-order errors of range position and implementing range pulse compression can be expressed as

$$Ss_i''(f_r, t; r) = W_r(f_r)\omega_a(t)\exp[-\frac{j4\pi(f_0+f_r)RI(t;r)}{c}] \tag{14}$$

D. ARRANGE THE SIGNAL IN THE AZIMUTH DIRECTION

Assume that the multiple-receiver SAS system has N receivers, and the sampling rate of each receiver is PRF. If the condition $v \big/ PRF = ND_r$ (D_r is the length of receiver) is satisfied, the echo signal from those N receivers can be converted into the monostatic SAS equivalents, by arranging those signals in the azimuth direction, whose sampling rate is $N \times PRF$. At this stage, the slow time t changes to t', but for simplicity, the variable t is still used.

E. AZIMUTH FFT

Utilizing the principle of stationary phase, the monostatic SAS signal could be transformed into azimuth frequency domain, which can be expressed as

$$\begin{aligned} SS_i''(f_r, f_a; r) = {} & W_r(f_r)W_a(f_a)\exp(j\frac{2\pi f_a r}{c}) \\ & \times \exp(j\frac{\pi f_a u_i}{v}) \\ & \times \exp[-j\frac{2\pi r}{vc}\sqrt{4v^2(f_c+f_r)^2 - (cf_a)^2}] \end{aligned} \tag{15}$$

where f_a is the frequency variable corresponding to slow time, and $W_a(f_a)$ is the Fourier transform of the antenna weighting.

The second phase term of (15) has been processed in the procedure of arranging the echo signal in the azimuth direction, which can be ignored in the follow derivation. Expand the third phase term of (15) in a power series at f_r, and keep terms up to f_r^2, then we get

$$\begin{aligned} SS(f_r, f_a; r) = {} & W_r(f_r)W_a(f_a)\exp(-j\frac{4\pi r f_0 D}{c}) \\ & \times \exp(-j\frac{4\pi r}{cD}f_r)\exp(j\frac{crf_a^2}{2v^2f_0^3D^3}f_r^2) \\ & \exp(j\frac{2\pi f_a r}{c}) \end{aligned} \tag{16}$$

$$D = \sqrt{1 - \frac{c^2 f_a^2}{4v^2 f_0^2}} \tag{17}$$

where the subscript i has been omitted.

F. BULK RCMC AND SRC

The bulk RCMC and second range compression (SRC) can be done with a phase multiplication in two-dimensional frequency domain. The phase multiplication is

$$H_3 = \exp(j\frac{4\pi r_{ref}}{cD}f_r)\exp(-j\pi\frac{cr_{ref}f_a^2}{2v^2f_0^3D^3}f_r^2) \tag{18}$$

where r_{ref} represents the reference slant range.

After the phase multiplication, the signal can be expressed as

$$\begin{aligned} SS'(f_r, f_a; r) = {} & W_r(f_r)W_a(f_a)\exp(-j\frac{4\pi r f_0 D}{c}) \\ & \times \exp[-j\frac{4\pi(r-r_{ref})}{cD}f_r]\exp(j\frac{2\pi f_a r}{c}) \end{aligned} \tag{19}$$

The signal trajectories after bulk RCMC is shown by the red dashed line in Fig. 4. The range curvature effect at reference range has been corrected completely, so the signal trajectory is a straight line. But differential range cell migration still exists at non-reference range, so the signal trajectories are curves.

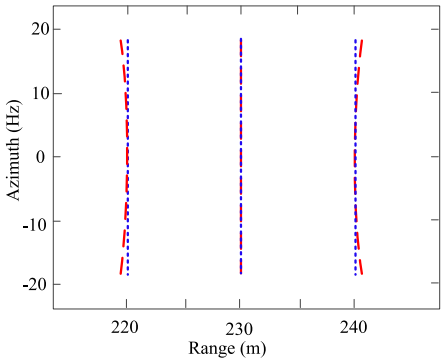

FIGURE 5. The signal trajectories in the range Doppler domain after chirp-z transform.

G. CHIRP-Z TRANSFORM

Assume that the sampling frequency in the range direction is f_s and the sampling number is N_r, then the discrete form of equation (19) is

$$SS'(k, f_a; l) = W_r(k)W_a(f_a)\exp(-j\frac{2\pi}{N_r D}kl) \times \exp[-j(\frac{4\pi f_0 D}{c} - \frac{2\pi f_a}{c})(r_{ref} + \frac{c}{2f_s}l)] \quad (20)$$

$$k = -\frac{N_r}{2}, \cdots, 0, 1, \cdots, \frac{N_r}{2} - 1 \quad (21)$$

$$l = -\frac{N_r}{2}, \cdots, 0, 1, \cdots, \frac{N_r}{2} - 1 \quad (22)$$

In order to correct the range-variant differential range cell migration, variable-scale Fourier transform from frequency domain k to spatial domain l is implemented for $SS'(k, f_a; l)$, and the transform kernel is $\exp(j2\pi kl/N_r D)$. The specific process is as follows:

$$2kl = k^2 + l^2 - (k - l)^2 \quad (23)$$

$$sS'(l, f_a) = \frac{1}{N_r}\exp(j\frac{\pi}{N_r D}l^2) \times \sum_{k=0}^{N-1} SS'(k, f_a; l) \times \exp(j\frac{\pi}{N_r D}k^2)\exp[-j\frac{\pi}{N_r D}(k - l)^2] \quad (24)$$

That is to say, the two-dimensional discrete spectrum $SS'(k, f_a; l)$ is multiplied by $\exp(j\pi k^2/N_r D)$, then the result is convoluted with $\exp(-j\pi k^2/N_r D)$, and then multiplied by $\exp(j\pi l^2/N_r D)$, where the convolution operation can be implemented quickly by FFT.

The signal after chirp-z transform can be expressed as

$$sS'(\tau, f_a) = \mathrm{sinc}[B_r(\tau - \frac{2r}{c})]W_a(f_a) \times \exp(-j\frac{4\pi r f_0 D}{c})\exp(j\frac{2\pi f_a r}{c}) \quad (25)$$

After chirp-z transform, the range cell migration in the whole swath is corrected completely, so the signal trajectories at any range are straight lines, which are shown by the blue dotted line in Fig. 5.

H. AZIMUTH FILTER AND AZIMUTH WALK CORRECTION

In the non-stop-hop-stop mode, the target in the focused image will have a slight azimuth offset from the ideal position, which is called azimuth walk and could be corrected with a phase multiplication. Azimuth walk correction can be combined with azimuth matched filtering, and the reference function is

$$H_4 = \exp(j\frac{4\pi f_0 D r}{c})\exp(-j\frac{2\pi f_a r}{c}) \quad (26)$$

I. AZIMUTH IFFT

The last step is an azimuth IFFT, and then we can obtain the focused image, which can be written as

$$ss'(\tau, t) = \mathrm{sinc}[B_r(\tau - \frac{2r}{c})]\mathrm{sinc}(B_a t) \quad (27)$$

where B_a is the Doppler bandwidth.

IV. POINT TARGET SIMULATION AND SEA TRIAL DATA PROCESSING

In this section, we present some simulations to review the imaging accuracy of the CZT algorithm. Based on the sea trial data, we compare the efficiency of the CS algorithm and CZT algorithm for multiple-receiver SAS.

A. POINT TARGET SIMULATION

In order to verify the effectiveness of the proposed algorithm, the simulation of different range point targets is carried out below, and the simulation parameters are shown in Table 1. In the scene, five point targets are set at near range, center range, and far range with coordinates of (220,25), (230,15), (230,25), (230,35), (240,25).

The imaging results processed by different algorithms are shown in Fig. 6. We observed that the two images, which are processed by CS algorithm and CZT algorithm respectively, are both focused well. The range and azimuth slices of the two images at different range are shown in Fig. 7(a)-(f), from which we can see that the range and azimuth slices processed by CZT algorithm and CS algorithm are almost identical, which shows that the imaging accuracy of the two algorithms are similar.

Table 2 is the image quality parameters processed by CZT algorithm, which can also represent that of CS algorithm as the imaging accuracy of the two algorithms are similar. The image quality is examined by impulse response

width (IRW), peak sidelobe ratio (PSLR) and integrated sidelobe ratio (ISLR). We observed from Table 2 that those parameters of the simulation results at range and azimuth direction are both close to the theoretical values, except the ISLR at azimuth direction, which are about 2 dB lower than the theoretical value due to the relatively large bandwidth. Based on those quantitative measures, the effectiveness of the proposed algorithm in imaging of multiple-receiver SAS can be demonstrated.

TABLE 2. Image quality parameters.

	Range			Azimuth		
	IRW (m)	PSLR (dB)	ISLR (dB)	IRW (m)	PSLR (dB)	ISLR (dB)
Theoretical Value	0.038	-13.3	-10.0	0.08	-13.3	-10.0
Near Range	0.038	-13.0	-10.1	0.083	-13.5	-11.8
Centre Range	0.038	-13.4	-10.5	0.077	-13.6	-12.0
Far Range	0.039	-12.8	-10.1	0.081	-13.9	-11.9

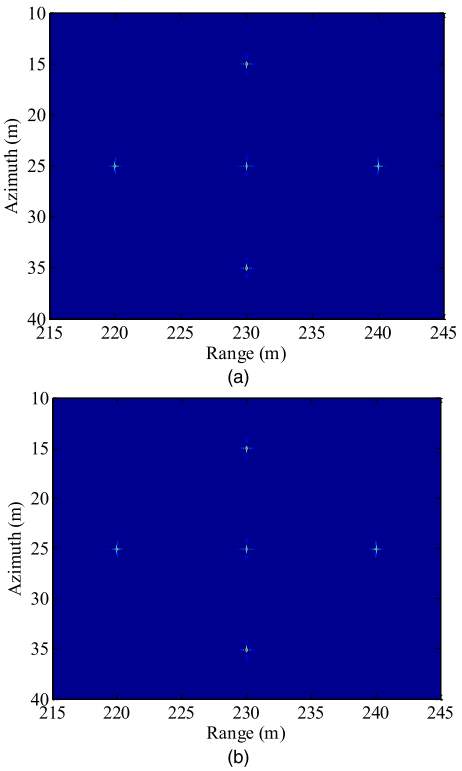

FIGURE 6. The imaging results processed by different algorithms (a) CS algorithm, (b) CZT algorithm.

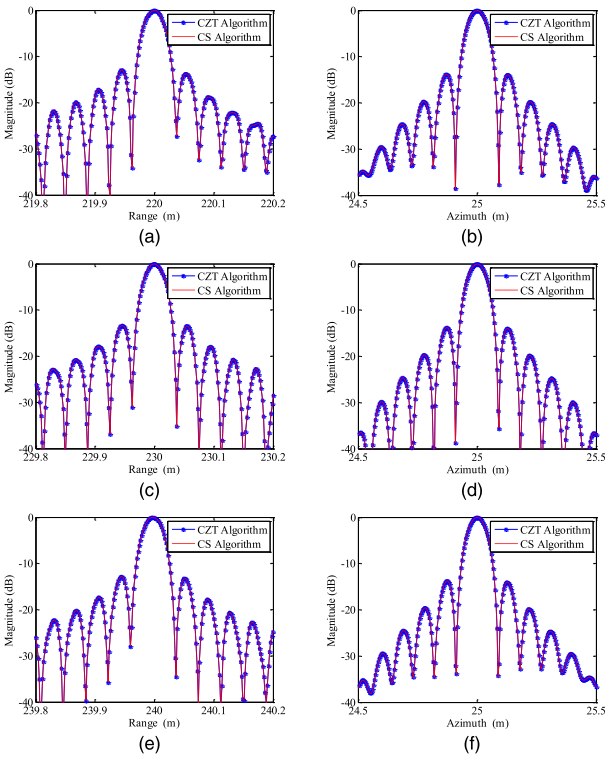

FIGURE 7. The range and azimuth slices of different range point targets processed by different algorithms (a) (b) The range and azimuth slices at near range, (c) (d) The range and azimuth slices at centre range, (e) (f) The range and azimuth slices at far range.

B. SEA-TRIAL DATA PROCESS

The parameters of sea-trial are the same as those of simulation, as shown in Table 1 again. The sea-trial data are processed in the following environment: processor Intel (R) Core (TM) i3-3240 CPU @ 3.40 GHz; memory 8 G; operating system Windows 7; professional 64-bit; software environment Matlab 2010b.

The sea-trial data points are 12000 in the range direction and 2520 in the azimuth direction. No weighting was used in either range or azimuth directions during the imaging processing. Fig. 8 (a) and Fig. 8 (b) is the images processed respectively by CS algorithm and CZT algorithm. Both of the two images are focused well as the sand dunes on the sea floor are clearly visible. Comparing the two images, it can be found that the image clarity and brightness changes are almost identical. In order to observe the details of the images, three partial zoomed plots at near, center, and far range of Fig. 8(a) is shown in Fig. 8 (c)-(e) and those of Fig. 8(b) is shown in Fig. 8 (f)-(h). Even for these partial zoomed plots, there is no difference between the two algorithms. So the CZT algorithm has the same focusing ability as CS algorithm, which proves the effectiveness of the proposed algorithm in multiple-receiver SAS imaging.

The average time taken for three imaging processes of CS algorithm is 27.6 s, and that of CZT algorithm is 24.2 s. It is worth noting that the range pulse compression is performed firstly during the imaging processing, which is necessary for removing the motion errors in the motion compensation. As the CS algorithm cannot process the pulse-compressed data, the decompression operation has been added, but the CZT algorithm is not affected, and still executed according to the flow of Fig. 2. So when combined with motion compensation, the CZT algorithm is slightly more efficient.

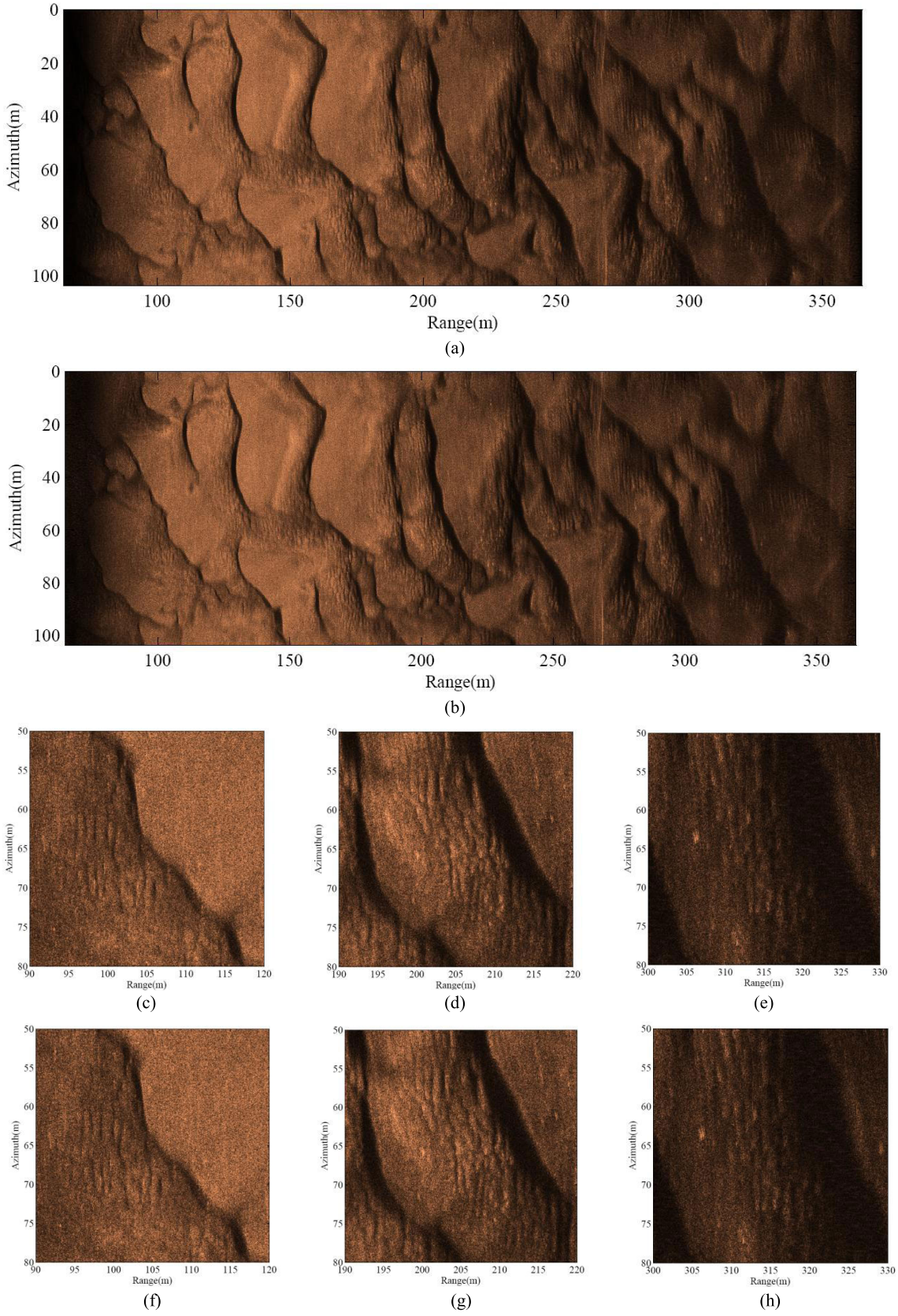

FIGURE 8. The imaging results of sea trial data. (a) Image processed by CS algorithm, (b) Image processed by CZT algorithm, (c),(d),(e) partial zoomed plots of (a) at near, centre, and far range, (f),(g),(h) partial zoomed plots of (b) at near, centre, and far range.

V. CONCLUSION

According to the geometry of multiple-receiver SAS, the echo range history model is given, and the CZT algorithm flow of multiple-receiver SAS is deduced. The point targets simulation and sea trial data process show that the imaging accuracy of multiple-receiver SAS CZT algorithm is equivalent to that of CS algorithm. As far as efficiency is concerned, the efficiency of multiple-receiver SAS CZT algorithm is lower than that of CS algorithm, but CZT algorithm can process the signal after range pulse compression directly, so when combined with motion compensation, CZT algorithm is slightly more efficient. Besides, CZT algorithm can process the non-LFM signal directly.

REFERENCES

[1] D. J. Sun and T. Tian, "The study of synthetic aperture sonar (SAS) technique (review)," *J. Harbin Eng. Univ.*, vol. 21, no. 1, pp. 51–56, Feb. 2000.
[2] R. E. Hansen, H. J. Callow, T. O. Sabo, and S. A. V. Synnes, "Challenges in seafloor imaging and mapping with synthetic aperture sonar," *IEEE Trans. Geosci. Remote Sens.*, vol. 49, no. 10, pp. 3677–3687, Oct. 2011.
[3] B. L. Douglas and H. Lee, "Synthetic-aperture sonar imaging with a multiple-element receiver array," in *Proc. IEEE Int. Conf. Acoust., Speech, Signal Process.*, Minneapolis, MN, USA, Apr. 1993, pp. 445–448.
[4] M. P. Hayes and P. T. Gough, "Synthetic aperture sonar: A review of current status," *IEEE J. Ocean. Eng.*, vol. 34, no. 3, pp. 207–224, Jul. 2009.
[5] I. G. Cumming and F. H. Wong, *Digital Processing of Synthetic Aperture Radar Data: Algorithms and Implementation*. Norwood, MA, USA: Artech House, 2005, pp. 154–245.
[6] H. J. Callow, "Signal processing for synthetic aperture sonar image enhancement," Ph.D. dissertation, Dept. Elec. Eng., Univ. Canterbury, Christchurch, New Zealand, 2003.
[7] X. B. Zhang, J. S. Tang, S. Zhang, S. X. Bai, and H. P. Zhong, "Four-order polynomial based range-Doppler algorithm for multi-receiver synthetic aperture sonar," *J. Electron. Inf. Technol.*, vol. 36, no. 7, pp. 1592–1598, Jul. 2014.
[8] Z. Tian, J. Tang, H. Zhong, and S. Zhang, "Extended range Doppler algorithm for multiple-receiver synthetic aperture sonar based on exact analytical two-dimensional spectrum," *IEEE J. Ocean. Eng.*, vol. 41, no. 1, pp. 164–174, Jan. 2016.
[9] H. L. Yang, S. Zhang, J. S. Tang, and M. Chen, "Accurate range Doppler algorithm for multiple-receiver synthetic aperture sonar," *J. Data Acqu. Proc.*, vol. 25, no. 3, pp. 313–317, May 2010.
[10] X. Zhang, H. Huang, W. Ying, H. Wang, and J. Xiao, "An indirect range-Doppler algorithm for multireceiver synthetic aperture sonar based on Lagrange inversion theorem," *IEEE Trans. Geosci. Remote Sens.*, vol. 55, no. 6, pp. 3572–3587, Jun. 2017.
[11] X. Zhang, J. Tang, and H. Zhong, "Multireceiver correction for the chirp scaling algorithm in synthetic aperture sonar," *IEEE J. Ocean. Eng.*, vol. 39, no. 3, pp. 472–481, Jul. 2014.
[12] Z. Tian, J. S. Tang, S. Zhang, P. Hang, and H. P. Zhong, "Multiple-receiver synthetic aperture sonar imaging algorithm based on modified DPC approximation," *Tech. Acoust.*, vol. 34, no. 2, pp. 216–219, Apr. 2015.
[13] H. L. Yang, J. S. Tang, and K. Xu, "A wideband Chirp Scaling imaging algorithm of synthetic aperture sonar based on wide swath," *J. Harbin Eng. Univ.*, vol. 36, no. 1, pp. 73–77, Jan. 2015.
[14] X. B. Zhang, J. S. Tang, H. P. Zhong, and S. Zhang, "Wavenumber-domain imaging algorithm for wide-beam multi-receiver synthetic aperture sonar," *J. Harbin Eng. Univ.*, vol. 35, no. 1, pp. 93–101, Jan. 2014.
[15] H. J. Callow, M. P. Hayes, and P. T. Gough, "Wavenumber domain reconstruction of SAR/SAS imagery using single transmitter and multiple-receiver geometry," *Elect. Letter*, vol. 38, no. 7, pp. 336–338, Mar. 2002.
[16] R. D. Paulis, C. Prati, F. Rocca, S. Scirpoli, and S. Tebaldini, "Focusing synthetic aperture sonar (SAS) data with the Omega-K technique," in *Proc. IEEE Int. Geos. Remote Sens. Sym.*, Cape Town, South Africa, Jul. 2009, pp. 68–71.
[17] I. Cumming, Y. Guo, and F. Wong, "A comparison of phase-preserving algorithms for burst-mode SAR data processing," in *Proc. IEEE Int. Geos. Remote Sens. Symp.*, Singapore, Aug. 1997, pp. 731–733.
[18] R. Bamler, "A comparison of range-Doppler and wavenumber domain SAR focusing algorithms," *IEEE Trans. Geosci. Remote Sens.*, vol. 30, no. 4, pp. 706–713, Jul. 1992.
[19] R. K. Raney, H. Runge, R. Bamler, I. G. Cumming, and F. H. Wong, "Precision SAR processing using chirp scaling," *IEEE Trans. Geosci. Remote Sens.*, vol. 32, no. 4, pp. 786–799, Jul. 1994.
[20] R. Lanari, "A new method for the compensation of the SAR range cell migration based on the chirp z-transform," *IEEE Trans. Geosci. Remote Sens.*, vol. 33, no. 5, pp. 1296–1299, Sep. 1995.
[21] G. Franceschetti, R. Lanari, and E. S. Marzouk, "A new two-dimensional squint mode SAR processor," *IEEE Trans. Aerosp. Electron. Syst.*, vol. 32, no. 2, pp. 854–863, Apr. 1996.
[22] P. Zhou, S. Zhou, T. Xiong, Y. Li, and M. D. Xing, "A chirp-z transform imaging algorithm for missile-borne SAR with diving maneuver based on the method of series reversion," *J. Electron. Inf. Technol.*, vol. 32, no. 12, pp. 2861–2867, Dec. 2010.
[23] R. Lanari and G. Fornaro, "A short discussion on the exact compensation of the SAR range-dependent range cell migration effect," *IEEE Trans. Geosci. Remote Sens.*, vol. 35, no. 6, pp. 1446–1452, Nov. 1997.
[24] H. L. Yang, "Studies on imaging algorithm of multiple-receiver synthetic aperture sonar,"Ph.D. dissertation, Elecron. Eng. Dept., Naval Univ. Eng., Wuhan, China, 2009.
[25] W. Hughes, K. Gault, and G. J. Princz, "A comparison of the range-Doppler and chirp scaling algorithms with reference to RADARSAT," in *Proc. Int. Geosci. Remote Sens. Symp.*, Lincoln, NE, USA, May 1996, pp. 1221–1223.
[26] M. Ma, J. Tang, Z. Tian, and H. Zhong, "Trajectory deviations in narrow-beam SAS: Analysis and compensation," in *Proc. 11th Int. Conf. Image Signal, Biom. Eng. Info.*, Beijing, China, Oct. 2018.
[27] J. S. Tang, C. H. Zhang, and Q. H. Li, "Multi-aperture synthetic aperture sonar imaging algorithm," in *Proc. Acad. Forum Chin. Youth*, Beijing, China, Oct. 1999, pp. 235–239.
[28] J. Xu, J. S. Tang, and C. H. Zhang, "Multi-aperture synthetic aperture sonar imaging algorithm," *Signal Process.*, vol. 19, no. 2, pp. 157–160, Apr. 2003.
[29] A. Bellettini and M. A. Pinto, "Theoretical accuracy of synthetic aperture sonar micronavigation using a displaced phase-center antenna," *IEEE J. Ocean. Eng.*, vol. 27, no. 4, pp. 780–789, Oct. 2002.
[30] M. Younis, C. Fischer, and W. Wiesbeck, "Digital beamforming in SAR systems," *IEEE Trans. Geosci. Remote Sens.*, vol. 41, no. 7, pp. 1735–1739, Jul. 2003.

MENGBO MA received the B.S. degree in electronic engineering from the Naval University of Engineering, Wuhan, China, in 2015, where he is currently pursuing the Ph.D. degree in underwater acoustical engineering.

His current interest is in synthetic aperture sonar signal processing.

JINSONG TANG received the Ph.D. degree in electronic engineering from the Nanjing University of Aeronautics and Astronautics, Nanjing, China, in 1996.

He is currently a Professor with the Naval University of Engineering, Wuhan, China. His current research interests include synthetic aperture sonar (SAS), interferometric SAS, and underwater acoustic communication. He was honored in the list of the "100 Talents Programme" issued by the Chinese Academy of Sciences, in 1999.

HEPING ZHONG received the B.S. and M.S. degrees in computer science and technology from the Naval University of Engineering, Wuhan, China, in 2005 and 2007, respectively, and the Ph.D. degree in underwater acoustical engineering from the Naval University of Engineering, in 2011.

He is currently a Lecturer with the Naval University of Engineering. His current research interests include synthetic aperture radar (sonar) interferometry software development, interferometric signal processing, and parallel computing.